Synthesis and Structural Characterization of Multi-Molybdenum-Substituted Preyssler-type Phosphotungstates

Muh. Nur Khoiru Wihadi,[a,b] Terufumi Haioka,[a] Tatsuhiro Kojima,[c] Xavier López,[d] Tadaharu Ueda,[e,f] Tsuneji Sano,[a] and Masahiro Sadakane*[a]

Abstract: We report the synthesis of multi-Mo-substituted Preyssler-type phosphotungstates, $[P_5W_{30-x}Mo_xO_{110}Na(H_2O)]^{14-}$, with different amounts of incorporated Mo *via* the hydrothermal reactions of H_3PO_4, Na_2WO_4, and Na_2MoO_4; and characterization by ^{31}P nuclear magnetic resonance (NMR), Fourier-transform infrared (FT-IR), elemental analysis, electrospray ionization-mass spectrometry (ESI-MS), and cyclic voltammetry. The number of substituted Mo increases by increasing the amount of Na_2MoO_4 in the reaction mixture, and in the $[P_5W_{30-x}Mo_xO_{110}Na(H_2O)]^{14-}$, up to penta-Mo-substituted species can be produced as mixtures of isomers with different Mo numbers and Mo positions. Single crystal X-ray structure analysis and density functional theory calculation indicate that the most suitable substitution position is the belt position.

Introduction

Polyoxometalates (POMs) are an interesting family of anionic metal-oxide molecules constructed mainly using early transition metals, such as W, Mo, V, and Nb in high oxidation states. The POM family exhibits properties such as multi-electron redox activity, acidic property, photochemistry, and magnetism, and has been applied in many fields of functional materials, such as catalysts, conducting materials, and magnetic materials.[1,2] Among the wide class of POMs, Preyssler-type phosphotungstates have been attracting significant attention, and they have been applied as catalysts,[3–12] single-molecule electret materials,[13] single-molecule magnetic materials,[14] conductive materials,[15–23] staining reagents,[24] antitumor activity,[25] liposome collapse reagents,[26] and antibacterial agents.[27–30] The Preyssler-type phosphotungstates, $[P_5W_{30}O_{110}Z^{n+}(H_2O)]^{(15-n)-}$, are constructed using five PO_4 tetrahedra surrounded by thirty WO_6 octahedra, which create a doughnut-shaped structure with an internal cavity space that can encapsulate a cation (Z^{n+}) in the molecule (Figure 1). Cations such as Na^+,[31,32] lanthanide,[4,13,33–36] actinide cations,[33–35,37-38] Ca^{2+},[4,33,37,39] Y^{3+},[4,33,37] Bi^{3+},[4,19,21,33,39] Ag^+,[28–30,40–42] or K^+,[5,6,43–45] can be encapsulated, and the replacement of the encapsulated cation is widely used to tune the properties of the Preyssler compound.

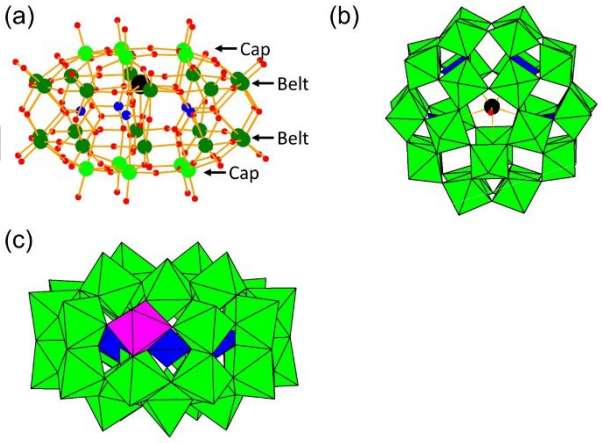

Figure 1. (a) Ball-and-stick and (b) polyhedral representation of the Preyssler-type phosphotungstate, $[P_5W_{30}O_{110}Na(H_2O)]^{14-}$, with one encapsulated Na and water oxygen; (c) polyhedral representation of mono-Mo-substituted Preyssler-type phosphotungstate where one Mo occupies the belt position; light green, dark green, red, and black balls represent tungstens on the cap position, tungstens on the belt position, oxygen, and encapsulated Na, respectively. Green octahedra, blue tetrahedra, and purple octahedron represent, WO_6 octahedra, PO_4 tetrahedra, and MoO_6 octahedra, respectively.

An alternative method to tune the properties is the substitution of framework W atoms. Pope et al. have reported mono-V-substituted species, $[P_5W_{29}VO_{110}Na]^{15-}$, which is prepared by a reaction of $VOSO_4$ with a lacunary Preyssler

[a] Dr. M. N. K. Wihadi, T. Haioka, Prof. Dr. T. Sano, Prof. Dr. M. Sadakane*
Department of Applied Chemistry
Graduate School of Advanced Science and Engineering, Hiroshima University
1-4-1 Kagamiyama, Higashi-Hiroshima 739-8527, Japan. Fax: +81 82 424 5494; Tel: +81 82 424 4456
E-mail: sadakane09@hiroshima-u.ac.jp
Homepage URL: home.hiroshima-u.ac.jp/catalche
[b] Dr. M. N. K. Wihadi
Research Center for Chemisty
National Research and Innovation Agency Republic of Indonesia
Kawasan Puspiptek, Serpong, Tangerang Selatan 15311, Indonesia
[c] Prof. Dr. T. Kojima
Department of Chemistry
Graduate School of Science, Osaka University
1-1, Machikaneyama, Toyanaka, Osaka, 560-0043, Japan
[d] Prof. Dr. X. López
Departament de Química Física i Inorgànica
Universitat Rovira i Virgili
c/Marcel·lí Domingo 1, 43007 Tarragona, Spain
[e] Prof. Dr. T. Ueda
Department of Marine Resource Science
Faculty of Agriculture and Marine Science, Kochi University
Nankoku, 780-8520, Japan
[f] Prof. Dr. T. Ueda
Center for Advanced Marine Core Research, Kochi University
Nankoku, 783-8502, Japan

Supporting information for this article is given via a link at the end of the document.

produced by reacting $[P_5W_{30}O_{110}Na]^{14-}$ with NaOH.[31] Amini et al. have reported a mono-Mo-substituted derivative, $[P_5W_{29}MoO_{110}Na]^{14-}$, by a hydrothermal reaction of H_3PO_4, Na_2WO_4, and Na_2MoO_4 in water.[46] Several research groups of Bamoharram,[7] Amini,[46] Ruiz[47] and Vázquez[48] have reported the improved catalytic activities of $[P_5W_{29}MoO_{110}Na(H_2O)]^{14-}$ for esterification and oxidation reactions. Recently, Schimpf et al. have reported that the iron-salt of $[P_5W_{29}MoO_{110}Na]^{14-}$ shows higher conductivities than the non-substituted $[P_5W_{30}O_{110}Na]^{14-}$ derivative.[22] They have reported the single crystal structure analysis of the K salt of $[P_5W_{29}MoO_{110}Na]^{14-}$ where the Mo substitution occurs on the belt position. Therefore, the design of Mo-substituted Preyssler derivatives is important. To the best of our knowledge, no information about multi-Mo-substituted derivatives has been reported.

Herein, we report the preparation and characterization of multi-Mo substituted Preyssler-type phosphotungstates, $[P_5W_{30-x}Mo_xO_{110}Na(H_2O)]^{14-}$ by the hydrothermal reaction of designated concentrations of H_3PO_4, Na_2WO_4, and Na_2MoO_4.

Results and Discussion

Reaction Condition and Isolation

The hydrothermal reaction of sodium tungstate (Na_2WO_4) and phosphoric acid (H_3PO_4) with different amounts (W:Mo = 30:0, 27:3, 25:5, 22:8, 20:10, 17:13, 9:21, 3:27 or 0:30) of sodium molybdate (Na_2MoO_4) was performed (Table 1). After the reaction mixture was cooled to room temperature, precipitates were obtained when the Mo amount was lower than W:Mo = 20:10 (Table 1, No. 1−5). The ^{31}P nuclear magnetic resonance (NMR) of the reaction solutions (Figure S1) indicated that the signal of $[P_5W_{30}O_{110}Na(H_2O)]^{14-}$ at approximately −9.58 ppm was observed when the Mo amount was lower than W:Mo = 20:10 (Figure S1 (a)−(e), Table 1, No. 1−5). Dawson-type $[P_2W_{18}O_{62}]^{6-}$ and its substituted species $[P_2W_{18-x}Mo_xO_{62}]^{6-}$ were detected at the range from −11.55 to −12.65 ppm in the samples with Mo amount was lower than 9:21 (Figure S1 (a) –(g)), and no peaks between −8 and −15 ppm were not observed for samples with the W:Mo ratio of 3:27 and 0:30 (Figure S1 (h) and (i)). The characterization of the formed precipitates by infrared (IR) and ^{31}P NMR indicated that these solids were Dawson-type species $[P_2W_{18-x}Mo_xO_{62}]^{6-}$ (Figures S2 and S3)[49].

The common procedure to isolate and purify the Preyssler-type phosphotungstate is precipitation by KCl addition to the reaction mixture and the subsequent recrystallization of the precipitates. The ^{31}P NMR of the precipitates after the addition of KCl showed the signal for $[P_5W_{30}O_{110}Na(H_2O)]^{14-}$ at −9.34 ppm, the signal corresponding to the Dawson-type $[P_2W_{18}O_{62}]^{6-}$ at −12.33 ppm, the signals corresponding to the $[\alpha_2\text{-}P_2W_{17}MoO_{62}]^{6-}$ at −11.27 ppm and −12.29 ppm, the signals corresponding to the $[\alpha_1\text{-}P_2W_{17}MoO_{62}]^{6-}$ at −11.33 ppm and -12.23 ppm (Figure S4) [49]. Furthermore, the phosphate derivatives observed between −2 and 2 ppm were present in the precipitates as impurities. No Preyssler-type phosphotungstate species were detected with a low amount of W (Figure S4, samples with W:Mo = 0:30, 3:27 and 9:21).

To increase the purify of the Preyssler derivatives, we performed recrystallization with the assumption that the substitution of W^{6+} with Mo^{6+} did not affect the crystallization behavior of the Preyssler species. After the first recrystallization, phosphate contamination in the solid decreased, and the Dawson anion derivative was partially separated in the filtrate solution, as shown in the ^{31}P NMR (Figures S5 and S6). However, in this step, the Dawson anion and phosphate contamination still existed in the solid. Therefore, we performed the second recrystallization to enhance the purity of the Preyssler-type compounds (W:Mo = 30:0, 27:3, 25:5, 22:8, 20:10).

Table 1. Ratio of W and Mo in the hydrothermal reaction for the Preyssler-type compounds and Isolated products

	Reaction mixture[a]		After the reaction		Isolated product
No.	Na_2WO_4 [g] ([mmol])	Na_2MoO_4 [g] ([mmol])	Preyssler in solution[b]	Solid[c]	W:Mo ratio[d]
1.	32.32 (98.0)	0 (0)	Y	Y	
	W:Mo = 30:0				
2.	29.380 (89.1)	2.060 (8.5)	Y	Y	
	W:Mo = 27:3				W:Mo = 28.9:1.1
3.	26.440 (80.0)	4.120 (16.9)	Y	Y	
	W:Mo = 25:5				W:Mo = 27.9:2.1
4.	23.510 (71.2)	6.180 (25.6)	Y	Y	
	W:Mo = 22:8				W:Mo = 27.6:2.4
5.	20.570 (62.5)	8.240 (33.9)	Y	Y	
	W:Mo = 20:10				W:Mo = 26.4:3.6
6.	17.630 (53.4)	10.300 (42.5)	N	N	
	W:Mo = 17:13				
7.	8.820 (26.7)	16.470 (68.0)	N	N	
	W:Mo = 9:21				
8.	2.940 (8.9)	20.590 (85.0)	N	N	
	W:Mo = 3:27				
9.	0 (0)	22.650 (93.5)	N	N	
	W:Mo = 0:30				

[a] Na_2WO_4-$2H_2O$, Na_2MoO_4-$2H_2O$, and H_3PO_4 (85%, 26.5 mL) were mixed with water (30 mL) in a Teflon-liner autoclave, and heated at 125 °C for 24 h. [b]Y indicates that Preyssler compounds are detected by the ^{31}P NMR of the reaction solution after the hydrothermal reaction. [c]Y indicates that solid was obtained after cooling the reaction mixture to room temperature. [d]W:Mo ratio of the solid obtained after the 2nd recrystallization is estimated by inductively coupled plasma (ICP) spectroscopy.

After the second recrystallization, we obtained the solid without phosphate species and Dawson-type species when W:Mo ratio was 30:0, 27:3, 25:5, 22:8, and 20:10 (Figure 2). All undesired compounds remained in the filtrate solutions (Figure S7). The ^{31}P NMR spectra of the crystals revealed signals at −9.34 ppm assigned to $[P_5W_{30}O_{110}Na(H_2O)]^{14-}$ and several small signals at −8.47 ppm, −9.49 ppm and −9.70 ppm (Figure 2).

Structural Characterization by IR, Elemental Analysis, high-resolution-electrospray ionization-mass spectrometry (HR-ESI-MS), Single-crystal X-ray diffraction (XRD), Density functional theory (DFT) calculation, and Cyclic Voltammetry

The IR spectra of the solids showed characteristic bands for the Preyssler-type phosphotungstate, $[P_5W_{30-x}Mo_xO_{110}Na(H_2O)]^{14-}$ (Figure 3).

The elemental analyses revealed the formula $K_{13.0}Na_{1.0}[P_5W_{28.9}Mo_{1.1}O_{110}Na(H_2O)]$, $K_{12.5}Na_{1.5}[P_5W_{27.9}Mo_{2.1}O_{110}Na(H_2O)]$, $K_{13.0}Na_{1.0}[P_5W_{27.6}Mo_{2.4}O_{110}Na(H_2O)]$, and $K_{12.5}Na_{1.5}[P_5W_{26.4}Mo_{3.6}O_{110}Na(H_2O)]$ for the solids prepared by different Na_2WO_4:Na_2MoO_4 ratios of 27:3, 25:5, 22:8, and 20:10, respectively. The increase in the amount of Na_2MoO_4 in the reaction mixture increased the amount of Mo in the Preyssler species.

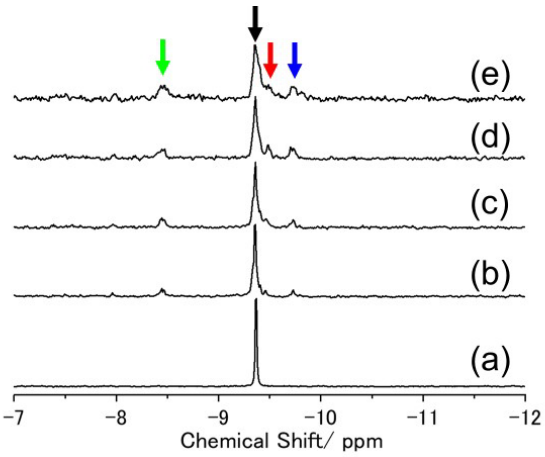

Figure 2. ^{31}P NMR spectra of the solid obtained after the 2nd recrystallization with different Na_2WO_4:Na_2MoO_4 ratios of (a) 30:0, (b) 27:3, (c) 25:5, (d) 22:8, and (e) 20:10 in the reaction mixture; the black arrow (-9.34 ppm) corresponds to $[P_5W_{30}O_{110}Na(H_2O)]^{14-}$. The green (−8.47 ppm), red (−9.49 ppm) and blue (−9.70 ppm) arrows correspond to $[P_5W_{30-x}Mo_xO_{110}Na(H_2O)]^{14-}$ with different numbers of Mo substitutions.

The isolated solids were analyzed by HR-ESI-MS after dissolving in H_2O–CH_3OH. For non-substituted Preyssler-type phosphotungatate, $[P_5W_{30}O_{110}Na(H_2O)]^{14-}$, profiles that correspond to a mixture of several Preyssler-type phosphotungstates were observed. The four most-intense profiles were assigned to $[H_8P_5W_{30}O_{110}K(H_2O)]^{6-}$, $[H_7KP_5W_{30}O_{110}Na(H_2O)]^{6-}$, $[H_7KP_5W_{30}O_{110}K(H_2O)]^{6-}$, and $[H_6K_2P_5W_{30}O_{110}Na(H_2O)]^{6-}$ (Figures S8(a), S9(a), and S10(a)). The mono-Na containing ions such as $[H_7KP_5W_{30}O_{110}Na(H_2O)]^{6-}$ and $[H_6K_2P_5W_{30}O_{110}Na(H_2O)]^{6-}$, were the proton-and-potassium mixed salts of the $[P_5W_{30}O_{110}Na(H_2O)]^{14-}$. Conversely, non-Na-containing ions, such as $[H_8P_5W_{30}O_{110}K(H_2O)]^{6-}$ and $[H_7KP_5W_{30}O_{110}K(H_2O)]^{6-}$ were K-encapsulated Preyssler compounds produced under ESI-MS conditions. The K-encapsulated Preyssler compound, $[P_5W_{30}O_{110}K(H_2O)]^{14-}$, has been reported by Sun et al.[44] We have reported that heating the K salt of Na-encapsulated anion, $K_{14}[P_5W_{30}O_{110}Na(H_2O)]$, produced mono-K- and di-K-encapsulated anions, such as $[P_5W_{30}O_{110}K]^{14-}$ and $[P_5W_{30}O_{110}K_2]^{14-}$.[45]

For the $[P_5W_{30-x}Mo_xO_{110}Na(H_2O)]^{14-}$, several profiles assignable to the Mo-substituted species were observed (Figures 4, S8, S9, and S10). The ESI-MS results of the $[P_5W_{28.9}Mo_{2.1}O_{110}Na(H_2O)]^{14-}$ showed profiles assignable to mono-Mo-, di-Mo-, and tri-Mo-substituted species (Figure 4 (a) and Figure S9(c)). Further, the more Mo-substituted species showed profiles assignable to more Mo-substituted species, and a penta-Mo-substituted complex was detected for $[P_5W_{26.4}Mo_{3.6}O_{110}Na(H_2O)]^{14-}$ (Figure 4 (b) and Figure S9 (e)).

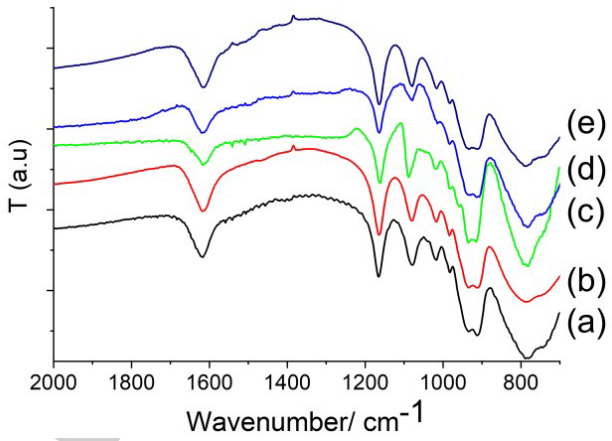

Figure 3 IR Spectra of the solid obtained after the 2nd recrystallization with different Na_2WO_4:Na_2MoO_4 ratios of (a) 30:0, (b) 27:3, (c) 25:5, (d) 22:8, and (e) 20:10 in the reaction mixture.

We conclude that we could isolate the mixtures of $[P_5W_{30-x}Mo_xO_{110}Na(H_2O)]^{14-}$ (x up to 5), owing to the following reasons. 1) Elemental analysis results showed P:W+Mo:K+Na atomic ratio was very close to 5:30:15 indicating that the K-Na mixed salts of the Preyssler-type compounds could be isolated. 2) ESI-MS spectra showed profiles assignable to the Mo-substituted Preyssler-type phosphotungstates (Figures 4, S8, S9, S10). 3) Although the ESI-MS profile indicated that they were mixtures with different Mo amounts, the formula of the most abundant Mo-substituted species was similar to that estimated by elemental analysis (Figure S9). 4) IR spectra showed characteristic band patterns for the Preyssler-type phosphotungstates (Figure 3). It is known that $H_3PW_{12}O_{40}$ and $H_3PMo_{12}O_{40}$ exhibited a similar IR patterns with different band positions.[50] In the present case, the maximum amount of Mo substituted in the Preyssler framework was 5, according to ESI-MS profiles (Figure 4 (b) and Figure S9(e)), and in such low Mo contents, the IR spectra of the Mo-substituted Preyssler compounds might be similar to that of the non-substituted $[P_5W_{30}O_{110}Na(H_2O)]^{14-}$.

Our results indicate that the mono-Mo-substituted derivative reported by Amini[46] and Schimpf[22] synthesized by the hydrothermal reaction of H_3PO_4, Na_2WO_4, and Na_2MoO_4 might be a mixture of several Preyssler-type phosphotungstates with different amounts of substituted Mo.

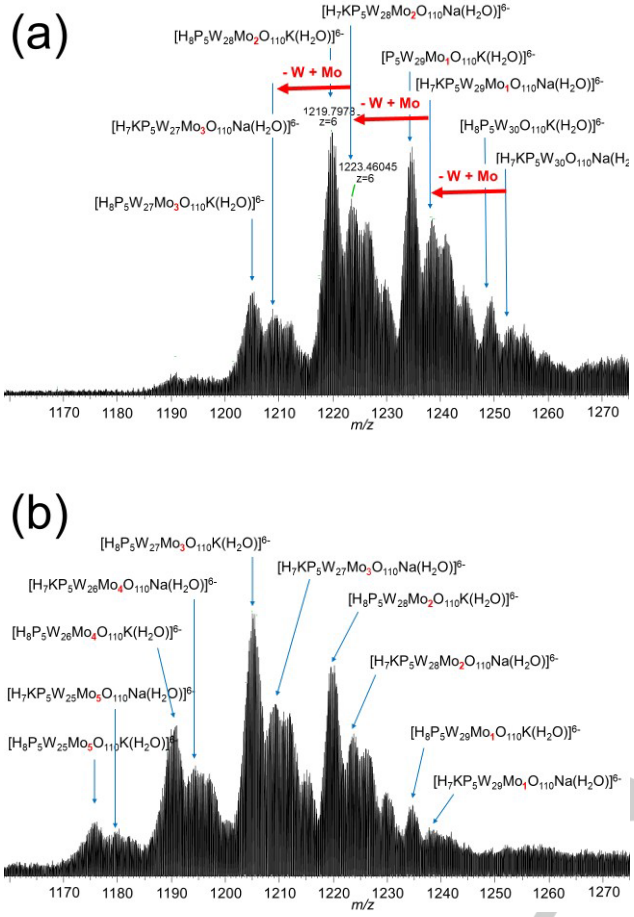

Figure 4. ESI-MS spectrum of (a) $K_{12.5}Na_{1.5}[P_5W_{27.9}Mo_{2.1}O_{110}Na(H_2O)]$ and (b) $K_{12.5}Na_{1.5}[P_5W_{24.6}Mo_{3.6}O_{110}Na(H_2O)]$ dissolved in H_2O–CH_3OH.

The ^{31}P NMR signal at −9.34 ppm, corresponding to the non-substituted $[P_5W_{30}O_{110}Na(H_2O)]^{14-}$, broadened and new peaks at −8.47, −9.47, and −9.70 ppm were observed after the introduction of Mo (Figure 2). The peak at -9.34 ppm broadened, and the intensities of the new peaks increased with the increase in the Mo amount, indicating that these signals were assignable to the Mo-substituted species. However, we could not assign all signals.

Five phosphorous in the non-substituted complex were equivalent, and therefore, only one ^{31}P NMR singlet is was observed. The ^{183}W NMR of the non-substituted complex showed four singlets because there were four kinds of W; cap W close to the encapsulated Na, cap W far from the encapsulated Na, belt W close to the encapsulated Na, and belt W far from the encapsulated Na.[4] The mono-Mo substitution of W produced four isomers, and there were three non-equivalent P in each isomer. Multi-Mo substitution produced more isomers and more non-equivalent P, thereby making the assignment of the ^{31}P NMR difficult.

Schimpf et al. have reported the single crystal structure analysis of K salt of $[P_5W_{29}MoO_{110}Na]^{14-}$, where the Mo substitution occurs on the belt position.[22] We performed the single crystal X-ray structure analysis of $K_{12.5}Na_{1.5}[P_5W_{26.4}Mo_{3.6}O_{110}Na(H_2O)]$. Similar to the single crystal X-ray structure analysis results of other Preyssler-compounds, $[P_5W_{26.4}Mo_{3.6}O_{110}Na(H_2O)]^{14-}$ crystalized in an *orthorhombic* unit cell with *Pnna* (52) space group and an asymmetric unit contained half of the Preyssler molecule, where cap and belt W close to Na were not distinguishable from those far from Na because of the disorder of the molecule (Figure S11). Our attempt to estimate the positions of Mo revealed that the W atoms, W_6−W_{15}, on the belt positions were subject to be substituted with Mo atoms rather than those, W_1−W_5, on the cap positions judging from the site occupancies of the W and Mo atoms. However, they were disordered over the belt positions (Table S1).

We performed a DFT study on the four isomers of the mono-Mo substituted compound (Table 2). The belt positions were the most stable for the W−Mo substitution. The belt substitution close to the encapsulated Na^+ (Entry 3) revealed higher stability than that far from the Na^+ but only by 0.74 kcal mol^{-1} (Entry 4). The two cap substitutions presented relatively high energies of 2.88 and 3.68 kcal mol^{-1} above the lowest energy form (Entries 1 and 2). These values evidenced the preference of the Mo for the belt positions.

Table 2. DFT calculation results for $[P_5W_{29}MoO_{110}Na]^{14-}$

Entry	Substitution Sites Model	Energy (kcal mol^{-1})	Relative energy (kcal mol^{-1})
1	Cap close to Na^+	−29892.51	2.9
2	Cap far from Na^+	−29891.71	3.7
3	Belt close to Na^+	−29895.39	0
4	Belt far from Na^+	−29894.65	0.74

Figure 5 shows the cyclic voltammogram (CV) of the $[P_5W_{30-x}Mo_xO_{110}Na(H_2O)]^{14-}$ series in 0.1 M HCl. The $[P_5W_{30}O_{110}Na(H_2O)]^{14-}$ exhibited two four-electron transfer processes and one two-electron transfer in 1.0 M HCl,[33,51] which appeared at −180 mV and −300 mV and −520 mV, respectively, in 0.1 M HCl. In the CVs of $[P_5W_{30-x}Mo_xO_{110}Na(H_2O)]^{14-}$ (Mo:W ratio = 3:27, 5:25, 8:22, and 10:20) new irreversible waves appeared at regions from -50 mV to +600 mV. Further, the current magnitude of waves increased depending on the amount of the substituted Mo, which is similar to the voltammetric behavior of Keggin-type $[PW_{12-x}Mo_xO_{40}]^{3-}$ (x = 1−11) formed in a 50 mM (W(VI)−Mo(VI)) – 10 mM P(V) – 0.5 M HCl – 50%(v/v) CH_3CN system.[52] These new waves corresponded to the redox of Mo(VI/V) in the Mo components of $[P_5W_{30-x}Mo_xO_{110}Na(H_2O)]^{14-}$, because the reduction potentials of the Mo components were more positive than those of the W components in POMs. Additionally, irreversible and broad-shaped waves showed that each of several Mo atoms in several isomers of $[P_5W_{30-x}Mo_xO_{110}Na(H_2O)]^{14-}$ generated from the incorporation of Mo at different positions of the framework of Preyssler-type POMs, could be reduced at different potentials.

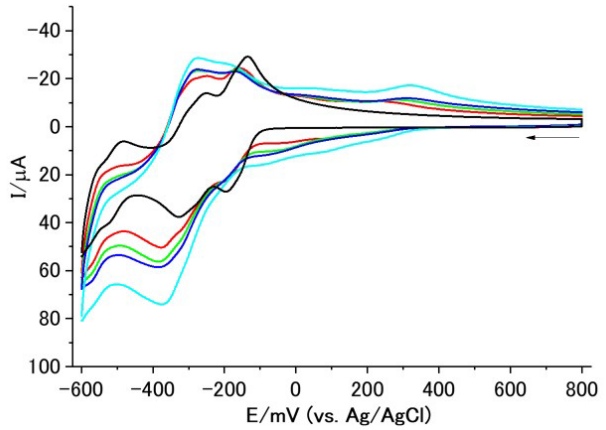

Figure 5. CVs of 0.5 mM (black) $K_{14}[P_5W_{30}O_{110}Na(H_2O)]$ (red) $K_{13.0}Na_{1.0}[P_5W_{28.9}Mo_{1.1}O_{110}Na(H_2O)]$, (green) $K_{12.5}Na_{1.5}[P_5W_{27.9}Mo_{2.1}O_{110}Na(H_2O)]$, (blue) $K_{13.0}Na_{1.0}[P_5W_{27.6}Mo_{2.4}O_{110}Na(H_2O)]$ and (cyan) $K_{12.5}Na_{1.5}[P_5W_{26.4}Mo_{3.6}O_{110}Na(H_2O)]$ in 0.1 M HCl; scan rate was 100 mVs^{-1}.

Conclusions

The first multi-Mo-substituted Preyssler-type phosphotungstates, $[P_5W_{30-x}Mo_xO_{110}Na(H_2O)]^{14-}$, have been successfully prepared *via* the self-assembly reaction of Na_2WO_4 and phosphoric acid with Na_2MoO_4 under hydrothermal conditions. The formation of $[P_5W_{30-x}Mo_xO_{110}Na(H_2O)]^{14-}$ and the number of Mo in the framework were dependent on the W:Mo ratio in the reaction medium. The Preyssler-type substituted framework was formed when the reaction conditions were in the range of 0 ≤ W:Mo ≤ 20:10. Further, Dawson-type substituted frameworks were found in the products when the reaction conditions were in the range of 0 ≤ W:Mo ≤ 9:21. Characterization by IR, ^{31}P NMR, elemental analysis, and ESI-MS confirmed that the isolated solids were a mixture of isomers of different numbers of incorporated Mo, possibly up to 5 molybdate atoms, into the framework to form $[P_5W_{25}Mo_5O_{110}Na(H_2O)]^{14-}$.

Experimental Section

Materials. Homemade deionized water (Millipore, Elix) was used. All chemicals were reagent-grade and used as provided.

Preparation of $K_{14}[P_5W_{30}O_{110}Na(H_2O)]-23H_2O$ (W:Mo = 30:0) $K_{14}[P_5W_{30}O_{110}Na(H_2O)]-23H_2O$ was prepared according to the published procedure[3,4,31]. Na_2WO_4-2H_2O (32.320 g, 98.0 mmol) was mixed with water (30 mL) in a Teflon-lined autoclave reactor, and phosphoric acid (85%, 26.5 mL) was added to the mixture. The reactor was placed in an oven heated at 125 °C for 24 h, and thereafter, the reactor was cooled to room temperature. A yellowish green crystal was obtained by filtration from the reaction mixture. The water (20 mL) was added to the filtrate, followed by KCl (10.0 g) addition, and the mixture was stirred for 10 min. The formed precipitates were filtered, and the solid was dried overnight at 70 °C (ca. 19.086 g). The solid was recrystallized from hot water (95 ºC, 40 mL) using a metal bath, and a white crystal was obtained by filtration (yield ca. 9.104 g). The solid was recrystallized again from 13 mL of hot water (95 ºC), and a pure white crystal was obtained by filtration (ca. yield 5.652 g, 0.670 mmol, 18.3 % based on W). IR (KBr): 1597.8 (m), 1162.9 (s), 1076.4 (s), 1019.2 (w), 912.1 (m), 785.9 (m) cm^{-1}. ^{31}P NMR (D_2O): −9.34 ppm. Negative ion MS (H_2O−CH_3OH): calcd. For $H_7K[P_5W_{30}O_{110}Na(H_2O)]^{6-}$ 1252.9775; found 1252.9747.

Preparation of $K_{13.0}Na_{1.0}[P_5W_{28.9}Mo_{1.1}O_{110}Na(H_2O)]-38H_2O$ (W:Mo = 27:3), $K_{12.5}Na_{1.5}[P_5W_{27.9}Mo_{2.1}O_{110}Na(H_2O)]-44H_2O$ (W:Mo = 25:5), $K_{13.0}Na_{1.0}[P_5W_{27.6}Mo_{2.4}O_{110}Na(H_2O)]-38H_2O$ (W:Mo = 22:8) and $K_{12.5}Na_{1.5}[P_5W_{26.4}Mo_{3.6}O_{110}Na(H_2O)]-46H_2O$ (W:Mo = 20:10) Na_2WO_4-2H_2O and Na_2MoO_4-2H_2O (29.380 g (89.1 mmol) and 2.060 g (8.5 mmol) for W:Mo = 27:3, 26.440 g (80.0 mmol) and 4.120 g (16.9 mmol) for W:Mo = 25:5, 23.510 g (71.2 mmol) and 6.180 g (25.5 mmol) for W:Mo = 22:8, and 20.570 g (62.9 mmol) and 8.240 g (33.9 mol) for W:Mo = 20:10) were mixed with water (30 mL) in a Teflon-lined autoclave reactor, and phosphoric acid (85%, 26.5 mL) was added to the mixture. The reactor was placed in an oven heated at 125 °C for 24 h, and thereafter, the reactor was cooled to room temperature. The yellowish green crystal was obtained by filtration from the reaction mixture. The water (20 mL) was added to the filtrate, KCl (10.0 g) was added, and the mixture was stirred for 10 min. The formed precipitates were filtered, and the solid was dried at 70 °C overnight to obtain a whitish green crude solid (ca. 4.02 g for W:Mo = 27:3, ca. 7.06 g for W:Mo = 25:5, ca. 9.6 g for W:Mo = 22:8, and ca. 9.88 g for W:Mo = 20:10). The solid was recrystallized from hot water (95 °C, 10 mL for W:Mo = 27:3, 15 mL for W:Mo = 25:5, 17 mL for W:Mo = 22:8, and 17 mL for W:Mo = 20:10) using a metal bath. The whitish green crystal was obtained by filtration (yield ca. 2.182 g for W:Mo = 27:3, ca. 4.14 g for W:Mo = 25:5, ca. 5.30 g for W:Mo = 22:8, and ca. 5.12 g for W:Mo = 20:10). The solid was recrystallized again from hot water (95 °C, 5 mL for W:Mo = 27:3, 7 mL for W:Mo = 25:5, 10 mL for W:Mo = 22:8, and 10 mL for W:Mo = 20:10) and the pure whitish green crystal was obtained by filtration.

$K_{13.0}Na_{1.0}[P_5W_{28.9}Mo_{1.1}O_{110}Na(H_2O)]-38H_2O$ (yield 1.075 g, 0.127 mmol, 3.6 % based on W): IR (KBr): 1618.5 (m), 1164.7 (s), 1079.0 (s), 1017.4 (w), 910.2 (m), 796.9 (m) cm^{-1}. ^{31}P NMR (D_2O): −8.47, −9.34, −9.49, and −9.70 ppm. Negative ion MS (H_2O-CH_3OH): calcd. For $H_7K[P_5W_{29}MoO_{110}Na(H_2O)]^{6-}$ 1238.1367; found 1238.1355. Elemental analysis: calculated: H 0.89, P 1.81, W 61.97, Mo 1.23, Na 0.54, K 5.93%; found H 0.69, P 1.81, W 62.07, Mo 1.34, Na 0.41, K 5.70%.

$K_{12.5}Na_{1.5}[P_5W_{27.9}Mo_{2.1}O_{110}Na(H_2O)]$ -45H_2O (yield 2.156 g, 0.251 mmol, 7.8 % based on W). IR (KBr): 1616.7 (m), 1161.9 (s), 1088.1 (s), 1019.4 (w), 934.6 (m), 782.1 (m) cm^{-1}. ^{31}P NMR (D_2O): −8.47, −9.34, −9.49, and −9.70 ppm. Negative ion MS (H_2O-CH_3OH): calcd. For $H_7K[P_5W_{29}MoO_{110}Na(H_2O)]^{6-}$ 1238.1367; found 1238.1359. Elemental analysis: calculated: H 1.05, P 1.80, W 59.62, Mo 2.34, Na 0.67, K 5.68%; found H 0.76, P 1.75, W 59.44, Mo 2.04, Na 0.54, K 5.50%.

$K_{13.0}Na_{1.0}[P_5W_{27.6}Mo_{2.4}O_{110}Na(H_2O)]-38H_2O$ (yield 2.123 g, 0.252 mmol, 8.6 % based on W). IR (KBr): 1619.6 (m), 1163.7 (s), 1079.5 (s), 1016.5 (w), 913.9 (m), 784.1 (m) cm^{-1}. ^{31}P NMR (D_2O): −8.47, −9.34, −9.49, and −9.70 ppm. Negative ion MS (H_2O-CH_3OH): calcd. For $H_7K[P_5W_{29}MoO_{110}Na(H_2O)]^{6-}$ 1238.1367; found 1238.1337. Elemental analysis: calculated: H 0.91, P 1.83, W 59.99, Mo 2.72, Na 0.54, K 6.01%; found H 0.63, P 1.77, W 59.93, Mo 2.72, Na 0.41, K 5.93%.

$K_{12.5}Na_{1.5}[P_5W_{26.4}Mo_{3.6}O_{110}Na(H_2O)]-46H_2O$ (yield 2.123 g, 0.250 mmol, 9.5 % based on W). IR (KBr): 1615.5 (m), 1163.9 (s), 1079.2 (s), 1016.4 (w), 932.6 (m), 786.6 (m) cm^{-1}. ^{31}P NMR (D_2O): −8.47, −9.34, −9.49, and −9.70 ppm. Negative ion MS (H_2O-CH_3OH): calcd. For $H_7K[P_5W_{29}MoO_{110}Na(H_2O)]^{6-}$ 1238.1367; found 1238.1334. Elemental analysis: calculated: H 1.09, P 1.82, W 57.17, Mo 4.07, Na 0.68, K 5.76%; found H 0.78, P 1.76, W 57.12, Mo 3.95, Na 0.42, K 5.80%.

Other analytical techniques. IR spectra were recorded on a NICOLET 6700 FT-IR spectrometer (Thermo Fisher Scientific) using KBr pellets. The ^{31}P NMR spectra were recorded on a Varian system 500 (500 MHz) spectrometer (Agilent) (P resonance frequency: 202.333 MHz). The spectra were referenced to external 85% H_3PO_4 (0 ppm). CV was performed on a CHI620D system (BAS Inc.) at ambient temperature. A glassy carbon working electrode (diameter, 3 mm), a platinum wire counter electrode, and an Ag/AgCl reference electrode (203 mV vs NHE at 25 °C) (3 M NaCl, BAS Inc.) were used. Elemental analyses were carried out at the Analysis Center at Mitsubishi Chemical Co. (Ootake, Japan). HR-ESI-MS spectra were recorded on an LTQ Orbitrap XL (Thermo Fisher Scientific) with an accuracy of 3 ppm. Each sample (5 mg) was dissolved in 5 mL of H_2O, and the solutions were diluted by CH_3OH (final concentration: ca. 10 μg/mL). All peak assignments were performed with an accuracy of less than 3 ppm.

Electronic Structure Calculations

DFT calculations were carried out on several isomers of the title structure using the ADF 2016 suite of programs.[53,54] Equilibrium geometries were obtained upon full geometry optimizations with tight convergence criteria[55] and the OPBE functional[56,57] with triple-ζ + double polarization atomic basis sets. The time-saving frozen core approximation was applied for the following atomic shells: 1s-2p for Na, 1s-2p for P, 1s-3d for Mo, 1s-4f for W and 1s for O. We simulated an aqueous solution (dielectric constant, ε = 78.4) by including the effects of solvent and counterions using the *conductor-like screening model* (COSMO).[58-61]

Single crystal X-ray diffraction analysis

Single crystals suitable for X-ray diffraction produced by the recrystallization of $K_{12.5}Na_{1.5}[P_5W_{26.4}Mo_{3.6}O_{110}Na(H_2O)]$ from hot water were selected using a microscope and mounted on a goniometer head using a LithoLoop. Intensity data were collected at 100 K on a Rigaku 1/4χ goniometer with a PILATUS3 X CdTe 1 M detector using synchrotron radiation (λ=0.4126 Å) monochromated by a Si (311) double crystal at SPring-8 (BL02B1 beamline). Data reduction was performed using RAPID AUTO. Absorption correction was performed by the multi-scan method implemented in ABSCOR. The structures were solved by direct methods using SHELXS-2014.[62] The structure was refined using full matrix least-squares (SHELXL-2018/3).[62] All non-hydrogen atoms were anisotropically refined. Hydrogen atoms on water molecules were not located. Global ISOR restraints were applied for O and P atoms. Each metal center at M_n (n = 6─15) was refined as two position-disordered metal ions (W_n/Mo_n) with free variable site occupancies, x and 1-x. The same refinement for M_n (n = 1─5) indicated that M_n (n = 1─5) was fully occupied by only W atom. EADP and EXYZ constraints were applied for these two disordered metal centers to fix atomic displacement parameters and coordinates, respectively. Twelve diffractions were omitted to improve the data quality. Crystallographic data were summarized in Table S2, and further details of the crystal structure investigation can be obtained from Fachinformationszentrum Karlsruhe, 76344 Eggenstein-Leopoldshafen, Germany (fax: +49-7247-808-666; e-mail: crysdata@fiz-karlsruhe.de; http://www.fiz-karlsruhe.de/request_for_deposited_data.html on quoting the deposition number CSD-2195592.

Acknowledgements

This research was supported by JSPS KAKENHI Grant Number JP21H02028 and JP18H02058 (Grant-in-aid for scientific research (B)), Grant-in-Aid for Transformative Research Area (A) "Supra-ceramics" (JSPS KAKENHI Grant Number JP22H05144), International Network on Polyoxometalate Science at Hiroshima University, JSPS Core-to-Core program, and Takahashi Industrial and Economic Research Foundation (12-003-147). MNKW gratefully acknowledges the financial support from the Indonesia Endowment Fund for Education (LPDP), Ministry of Finance, Republic of Indonesia for Ph.D. scholarship (PRJ-36/ LPDP.3/2017). XL is grateful for the financial support of the Spanish Government (grant nr. PID2020-112762GB-I00). We thank Ms. T. Amimoto at the Natural Science Center for Basic Research and Development (N-BARD), Hiroshima University, for the ESI-MS measurements. We thank Mitsubishi Chemical Co. for the ICP measurement. The synchrotron radiation experiment was performed on BL02B1 at Spring-8 with the approval of the Japan Synchrotron Radiation Research Institute (JASRI) (Proposal No. 2020 A1795).

Keywords: Polyoxometalate • Preyssler-type phosphotungstate • Substitution • Molybdate • Assembly

[1] M. T. Pope, *Heteropoly and Isopoly Oxometalates*, Springer-Verlag, Berlin, **1983**.

[2] (a) C. L. Hill, Thematic issue on Polyoxometalates, *Chem. Rev.* **1998**, *98*, 1–380; (b) L. Cronin, A. Müller, Thematic issue on Polyoxometalates, *Chem. Soc. Rev.* **2012**, *41*, 7333−7646.

[3] M. Sadakane, Y. Ichi, Y. Ide, T. Sano, *Z. Anorg. Allg. Chem.* **2011**, *637*, 2120–2124.

[4] K. Takahashi, T. Sano, M. Sadakane, *Z. Anorg. Allg. Chem.* **2014**, *640*, 1314–1321.

[5] A. Hayashi, H. Ota, X. López, N. Hiyoshi, N. Tsunoji, T. Sano, M. Sadakane, *Inorg. Chem.* **2016**, *55*, 11583-11592.

[6] A. Hayashi, M. N. K. Wihadi, H. Ota, X. López, K. Ichihashi, S. Nishihara, K. Inoue, N. Tsunoji, T. Sano, M. Sadakane, *ACS Omega* **2018**, *3*, 2363–2373.

[7] F. F. Bamoharram, M. M. Heravi, M. Roshani, M. Jahangir, A. Gharib, *J. Mol. Catal. A: Chem.* **2007**, *271*, 126–130.

[8] F. F. Bamoharram, M. M. Heravi, M. Roshani, M. Jahangir, A. Gharib, *Appl. Catal., A* **2006**, *302*, 42-47.

[9] M. M. Heravi, F. K. Behbahani, F. F. Bamoharram, *J. Mol. Catal. A: Chem.* **2006**, *253*, 16–19.

[10] M. M. Heravi, K. Bakhtiari, Z. Daroogheha, F. F. Bamoharram, *Catal. Commun.* **2007**, *8*, 1991-1994.

[11] R. Hekmatshoar, M. M. Heravi, S. Sadjadi, H. A. Oskooie, F. F. Bamoharram, *Catal. Commun.* **2008**, *9*, 837-841.

[12] N. Feizi, H. Hassani, M. Hakimi, *Bull. Korean Chem. Soc.* **2005**, *26*, 2087-2088.

[13] C. Kato, R. Machida, R. Maruyama, R. Tsunashima, X.-M. Ren, M. Kurmoo, K. Inoue, S. Nishihara, *Angew. Chem. Int. Ed.* **2018**, *57*, 13429-13432.

[14] S. Cardona-Serra, J. M. Clemente-Juan, E. Coronado, A. Gaita-Ariño, A. Camón, M. Evangelisti, F. Luis, M. J. Martínez-Pérez, J. Sesé, *J. Am. Chem. Soc.* **2012**, *134*, 14982–14990.

[15] M. Zhu, T. Iwano, M. Tan, D. Akutsu, S. Uchida, G. Chen, X. Fang, *Angew. Chem. Int. Ed.* **2022**, *61*, e202200666.

[16] T. Iwano, K. Shitamatsu, N. Ogiwara, M. Okuno, Y. Kikukawa, S. Ikemoto, S. Shirai, S. Muratsugu, P. G. Waddell, R. J. Errington, M. Sadakane, S. Uchida, *ACS Appl. Mater. Interfaces* **2021**, *13*, 19138–19147.

[17] A. Amini, M. Rahimi, M. Nazari, C. Cheng, B. Samali, *RSC Adv.* **2019**, *9*, 2772–2783.

[18] T. Iwano, S. Miyazawa, S. Uchida, *Inorg. Chim. Acta* **2020**, *499*, 119204-119210.

[19] T. Iwano, S. Miyazawa, R. Osuga, J. N. Kondo, K. Honjo, T. Kitao, T. Uemura, S. Uchida, *Commun. Chem.* **2019**, *2*, 9.

[20] S. Sun, L.-J. Zhu, K. Li, D.-M. Cheng, B. Li, Y.-H. Wang, H.-Y. Zang, Y.-G. Li, *Polyhedron* **2019**, *169*, 84–88.
[21] K. Niinomi, S. Miyazawa, M. Hibino, N. Mizuno, S. Uchida, *Inorg. Chem.* **2017**, *56*, 15187-15193.
[22] L. Chen, K. A. San, M. J. Turo, M. Gembicky, S. Fereidouni, M. Kalaj, A. M. Schimpf, *J. Am. Chem. Soc.* **2019**, *141*, 20261-20268.
[23] N. Ogiwara, T. Iwano, T. Ito, S. Uchida, *Coord. Chem. Rev.* **2022**, *462*, 214524.
[24] K. Sahiro, Y. Kawato, K. Koike, T. Sano, T. Nakai, M. Sadakane, *Sci. Rep.* **2022**, *12*, 7554.
[25] S. F. Razavi, F. F. Bamoharram, T. Hashemi, K. Shahrokhabadi, A. Davoodnia, *Toxicol in Vitro* **2020**, *68*, 104917.
[26] D. Kobayashi, Y. Ouchi, M. Sadakane, K. Unoura, H. Nabika, *Chem. Lett.* **2017**, *46*, 533–535.
[27] N. I. Gumerova, E. Al-Sayed, L. Krivosudský, H. Čipčić-Paljetak, D. Verbanac, A. Rompel, *Front. Chem.* **2018**, *6*, 336.
[28] K. Chen, Q. Yu, Y. Liu, P. Yin, *J. Inorg. Biochem.*, **2021**, *220*, 111463.
[29] A. Haider, K. Zarschler, S. A. Joshi, R. M. Smith, Z. Lin, A. S. Mougharbel, U. Herzog, C. E. Müller, H. Stephan, U. Kortz, *Z. Anorg. Allg. Chem.* **2018**, *644*, 752–758.
[30] B. Fan, N. Cui, Z. Xu, K. Chen, P. Yin, K. Yue, W. Tang, *Biomacromolecules* **2022**, *23*, 972–982.
[31] M. H. Alizadeh, S. P. Harmalker, Y. Jeannin, J. Martin-Frere, M. T. Pope, *J. Am. Chem. Soc.* **1985**, *107*, 2662-2669.
[32] M. N. K. Wihadi, A. Hayashi, T. Ozeki, K. Ichihashi, H. Ota, M. Fujibayashi, S. Nishihara, K. Inoue, N. Tsunoji, T. Sano, M. Sadakane, *Bull. Chem. Soc. Jpn.* **2020**, *93*, 461-466.
[33] I. Creaser, M. C. Heckel, R. J. Neitz, M. T. Pope, *Inorg. Chem.* **1993**, *32*, 1573-1578.
[34] M. H. Dickman, G. J. Gama, K.-C. Kim, M. T. Pope, *J. Cluster Sci.* **1996**, *7*, 567–583.
[35] C. W. Williams, M. R. Antonio, L. Soderholm, *J. Alloys Compd.* **2000**, *303–304*, 509–513.
[36] K. Shitamatsu, T. Kojima, P. G. Waddell, Sugiarto, H. E. Ooyama, R. J. Errington, M. Sadakane, *Z. Anorg. Allg. Chem.* **2021**, *647*, 1239–1244
[37] K. C. Kim, M. T. Pope, G. J. Gama, M. H. Dickman, *J. Am. Chem. Soc.* **1999**,*121*, 11164-11170.
[38] M. R. Antonio, M. H. Chiang, *Inorg. Chem.* **2008**, *47*, 8278-8285.
[39] A. Hayashi, T. Haioka, K. Takahashi, B. S. Bassil, U. Kortz, T. Sano, M. Sadakane, *Z. Anorg. Allg. Chem.* **2015**, *641*, 2670–2676.
[40] J. Du, M.-D. Cao, S.-L. Feng, F. Su, X.-J. Sang, L.-C. Zhang, W.-S. You, M. Yang, Z.-M. Zhu, *Chem. Eur. J.* **2017**, *23*, 14614–14622.
[41] M.-X. Liang, C.-Z. Ruan, D. Sun, X.-J. Kong, Y.-P. Ren, L.-S. Long, R.-B. Huang, L.-S. Zheng, *Inorg. Chem.* **2014**, *53*, 897-902.
[42] C. Kato, K. Y. Maryunina, K. Inoue, S. Yamaguchi, H. Miyaoka, A. Hayashi, M. Sadakane, R. Tsunashima, S. Nishihara, *Chem. Lett.* **2017**, *46*, 602–604.
[43] A.-X. Tian, Y. Yang, H.-P. Ni, G.-Y. Liu, Y.-B. Fu, M.-L. Yang, G.-C. Liu, J. Ying, Transition *Met. Chem.* **2018**, *44*, 303-309.
[44] T.-P. Hu, Y.-Q. Zhao, Z. Jaglič, K. Yu, X.-P. Wang, D. Sun, *Inorg. Chem.* **2015**, *54*, 7415–7423.
[45] M. N. K. Wihadi, M. Sadakane, *Z. Anorg. Allg. Chem.* **2020**, *646*, 1297-1302.
[46] M. Arabi, M. M. Amini, M. Abedini, A. Nemati, M. Alizadeh, *J. Mol. Catal. A: Chem.* **2003**, *200*, 105–110.
[47] D. M. Ruiz, G. P. Romanelli, P. G. Vázquez, J. C. Autino, *Appl. Catal., A.* **2010**, *374*, 110–119.
[48] G. Romanelli, D. Ruiz, P. Vázquez, H. Thomas, J. C. Autino, *Chem. Eng. J.* **2010**, *161*, 355-362.
[49] M. Abbessi, R. Contant, R. Thouvenot, G. Herve, *Inorg. Chem.* **1991**, *30*, 1695–1702.
[50] U. B. Mioč, M. R. Todorović, M. Davidović, P. Colomban, I. Holclajtner-Antunović, *Solid State Ionics* **2005**, *176*, 3005–3017.
[51] M.-H. Chiang, M. R. Antonio, L. Soderholm, *Dalton Trans*. **2004**, 3562-3567.
[52] T. Ueda, T. Toya, M. Hojo, *Inorg. Chim. Acta* **2004**, *357*, 59-65.
[53] C. Fonseca Guerra, J. G. Snijders, G. Te Velde, E. J. Baerends, *Theor. Chem. Acc.* **1998,** *99*, 391-403.
[54] G. te Velde, F. M. Bickelhaupt, E. J. Baerends, C. Fonseca Guerra, S. J. A. van Gisbergen, J. G. Snijders, T. Ziegler, *J. Comput. Chem.* **2001,** *22*, 913-967.
[55] Optimized structures must be very accurate when frequency calculations are to be conducted since molecular vibrations can be highly dependent on geometrical parameters.
[56] N. C. Handy, A. J. Cohen, *Mol. Phys.* **2001,** *99*, 403-412.
[57] M. Swart, A. W. Ehlers, K. Lammertsma, *Mol. Phys.* **2004,** *102*, 2467-2474.
[58] A. Klamt, G. Schüürmann, *J. Chem. Soc., Perkin Trans. 2* **1993,** *2*, 799-805.
[59] J. Andzelm, C. Kölmel, A. Klamt, *J. Chem. Phys.* **1995,** *103*, 9312
[60] A. Klamt, *J. Phys. Chem.* **1995,** *99*, 2224-35.
[61] C. C. Pye, T. Ziegler, *Theor. Chem. Acc.* **1999,** *101*, 396-408.
[62] G. M. Sheldrick, *Acta Crystallogr., Sect. A: Found. Adv.* **2008**, *A64*, 112–122.

Entry for the Table of Contents (Please choose one layout)

Layout 2:

FULL PAPER

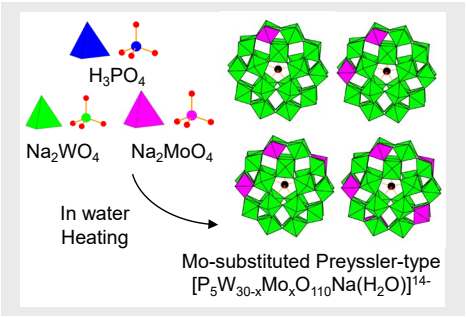

Key Topic*

*M. N. K. Wihadi, T. Haioka, T. Kojima, X. López, T. Ueda, T. Sano, M. Sadakane**

Page No. – Page No.

Synthesis and Structural Characterization of Multi-Molybdenum-Substituted Preyssler-type Phosphotungstates

The reaction of Na_2WO_4 and Na_2MoO_4 with H_3PO_4 produces multi-Mo-substituted Preyssler-type phosphotungstate, $[P_5W_{30-x}Mo_xO_{110}Na(H_2O)]^{14-}$ (x up to 5).

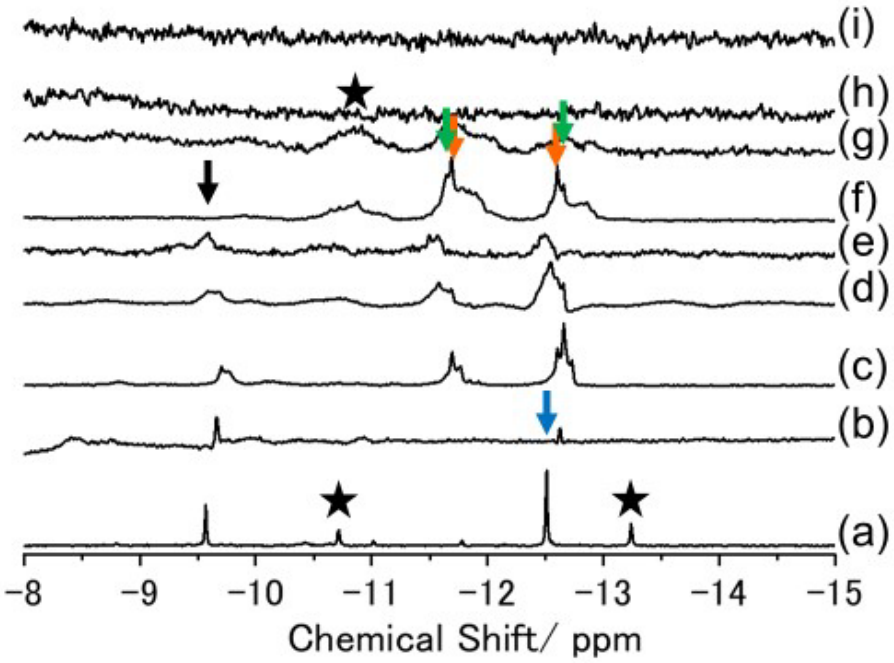

Figure S1. ^{31}P NMR spectra of the parent solution after hydrothermal reaction with different Na_2WO_4:Na_2MoO_4 ratios of (a) 30:0, (b) 27:3, (c) 25:5, (d) 22:8, (e) 20:10, (f) 17:13, (g) 9:21, (h) 3:27, and (i) 0:30 in the reaction mixture; the black, blue, orange, and green arrows correspond to $[P_5W_{30}O_{110}Na(H_2O)]^{14-}$, $[P_2W_{18}O_{62}]^{6-}$, $[\alpha_2\text{-}P_2W_{17}MoO_{62}]^{6-}$, and $[\alpha_1\text{-}P_2W_{17}MoO_{62}]^{6-}$, respectively. The black stars correspond to the unknown species detected.

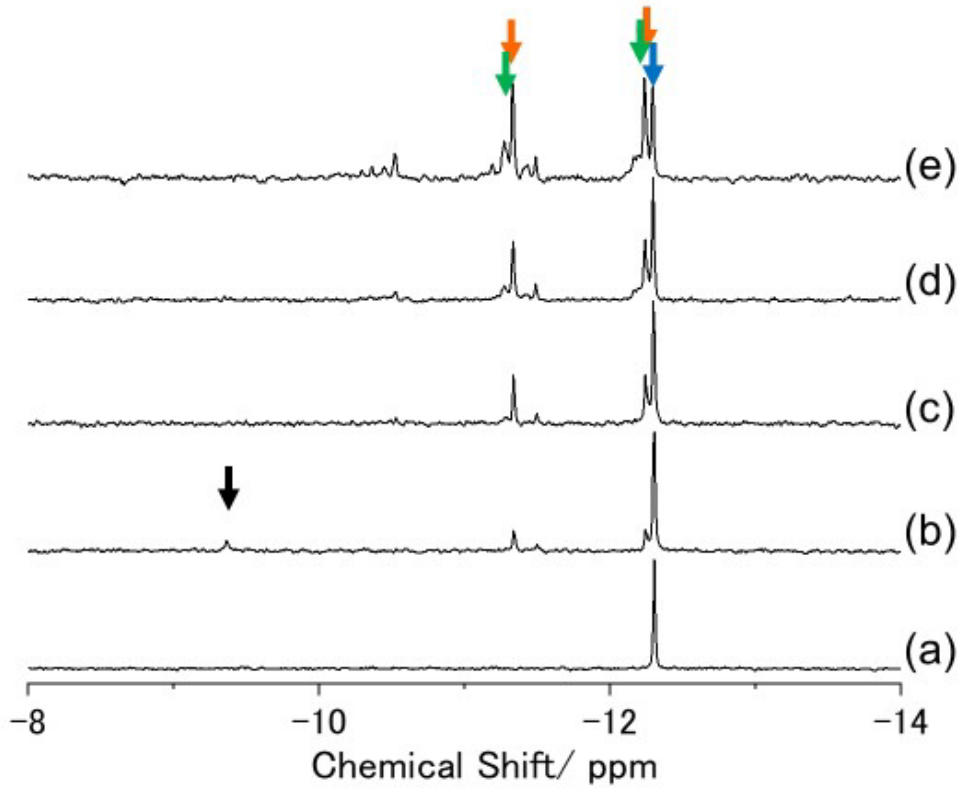

Figure S2. ^{31}P NMR spectra of the solid obtained inside the reactor prepared with different Na_2WO_4:Na_2MoO_4 ratios of (a) 30:0, (b) 27:3, (c) 25:5, (d) 22:8, and (e) 20:10; no solid was found after the reaction when the Na_2MoO_4 amount was more than Na_2WO_4:Na_2MoO_4 ratio of 20:10. The black (−9.34 ppm), blue (−12.33 ppm), orange (−11.27 and −12.29 ppm) and green (−11.33 and −12.23 ppm) arrows correspond to $[P_5W_{30}O_{110}Na(H_2O)]^{14-}$, $[P_2W_{18}O_{62}]^{6-}$, $[\alpha_2$-$P_2W_{17}MoO_{62}]^{6-}$, and $[\alpha_1$-$P_2W_{17}MoO_{62}]^{6-}$, respectively.

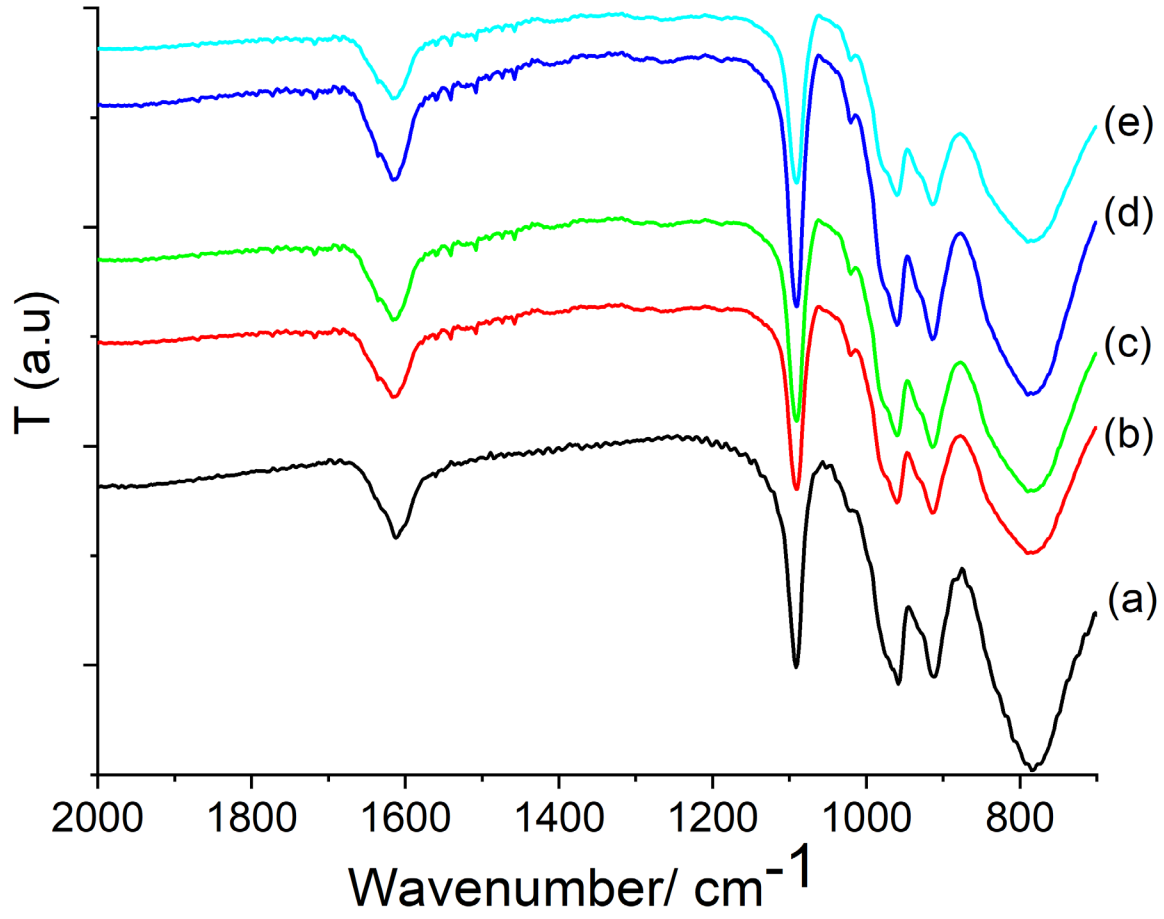

Figure S3. IR spectra of the solid obtained inside the reactor prepared with different Na_2WO_4:Na_2MoO_4 ratios of (a) 30:0, (b) 27:3, (c) 25:5, (d) 22:8, and (e) 20:10 in the reaction mixture; no solid was found after the reaction when the Na_2MoO_4 amount was more than Na_2WO_4:Na_2MoO_4 ratio of 20:10. Bands at ca. 1620 and 1095 cm^{-1} correspond to the vibration of H_2O and P−O, respectively. The bands between ca. 990 to 700 cm^{-1} correspond to the vibration of Mo−O. These band patterns are characteristic of a Dawson-type molecule.

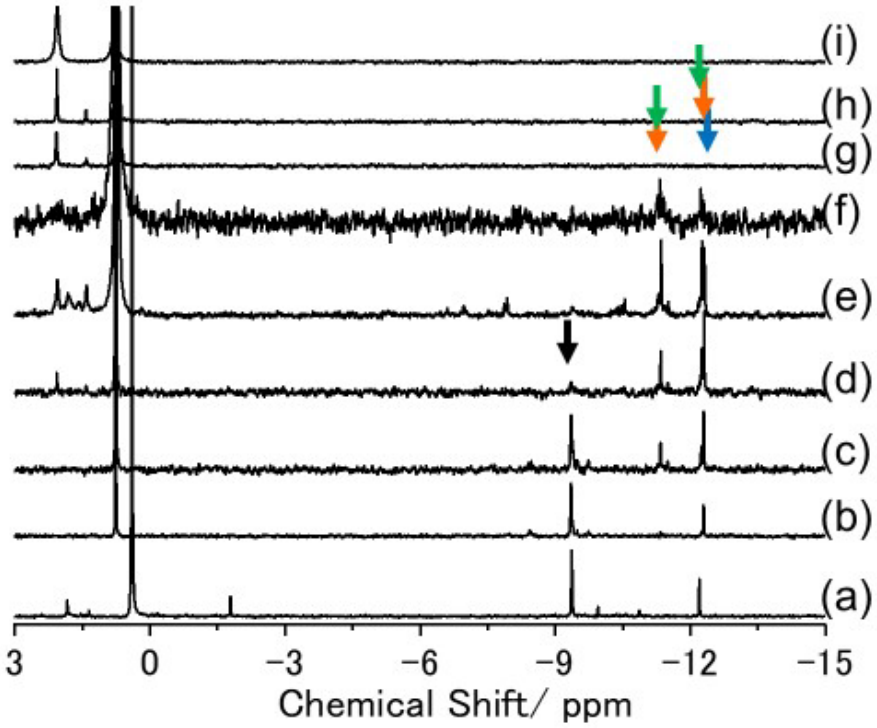

Figure S4. ^{31}P NMR spectra of the solids obtained by addition of KCl to the reaction solution prepared with different Na_2WO_4:Na_2MoO_4 ratios of (a) 30:0, (b) 27:3, (c) 25:5, (d) 22:8, (e) 20:10, (f) 17:13, (g) 9:21, (h) 3:27, and (i) 0:30 in the reaction mixture; the black (−9.34 ppm), blue (−12.33 ppm), orange (−11.27 and −12.29 ppm) and green (−11.33 and −12.23 ppm) arrows correspond to $[P_5W_{30}O_{110}Na(H_2O)]^{14-}$, $[P_2W_{18}O_{62}]^{6-}$, $[\alpha_2\text{-}P_2W_{17}MoO_{62}]^{6-}$, and $[\alpha_1\text{-}P_2W_{17}MoO_{62}]^{6-}$, respectively.

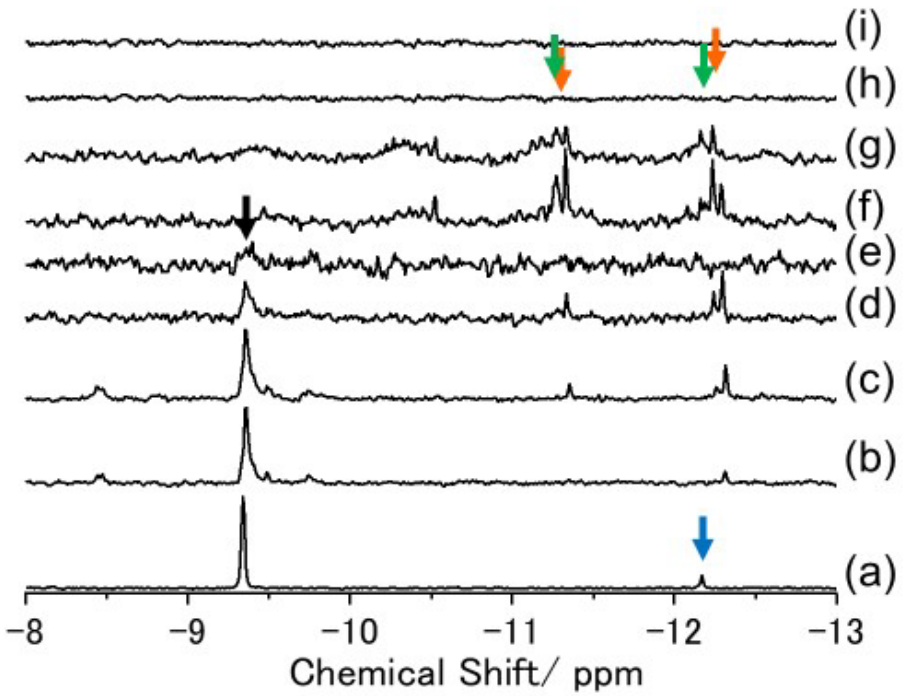

Figure S5. ^{31}P NMR Spectra of the solid obtained after the 1st recrystallization with different Na_2WO_4:Na_2MoO_4 ratios of (a) 30:0, (b) 27:3, (c) 25:5, (d) 22:8, (e) 20:10, (f) 17:13, (g) 9:21, (h) 3:27 and (i) 0:30 in the reaction mixture; the black (−9.34 ppm), blue (−12.33 ppm), orange (−11.27 and -12.29 ppm) and green (−11.33 and −12.23 ppm) arrows correspond to $[P_5W_{30}O_{110}Na(H_2O)]^{14-}$, $[P_2W_{18}O_{62}]^{6-}$, $[\alpha_2\text{-}P_2W_{17}MoO_{62}]^{6-}$, and $[\alpha_1\text{-}P_2W_{17}MoO_{62}]^{6-}$, respectively.

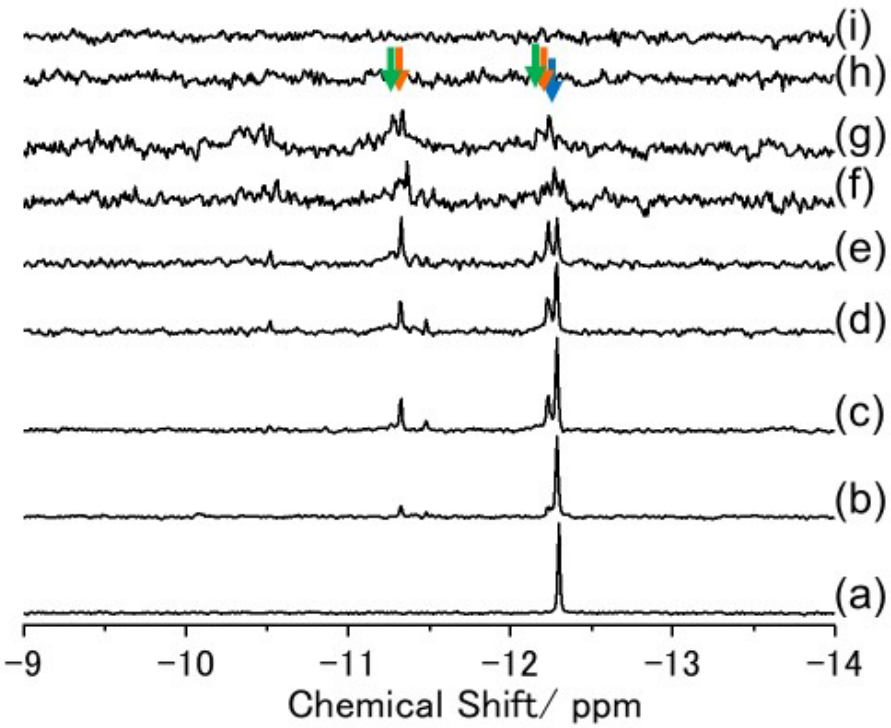

Figure S6. ^{31}P NMR spectra of the filtrate solution obtained after the 1st recrystallization with different Na_2WO_4:Na_2MoO_4 ratios of (a) 30:0, (b) 27:3, (c) 25:5, (d) 22:8, (e) 20:10, (f) 17:13, (g) 9:21, (h) 3:27, and (i) 0:30 in the reaction mixture; the blue (−12.33 ppm), orange (−11.27 and −12.29 ppm) and green (−11.33 and −12.23 ppm) arrows correspond to $[P_2W_{18}O_{62}]^{6-}$, $[\alpha_2$-$P_2W_{17}MoO_{62}]^{6-}$, and $[\alpha_1$-$P_2W_{17}MoO_{62}]^{6-}$, respectively.

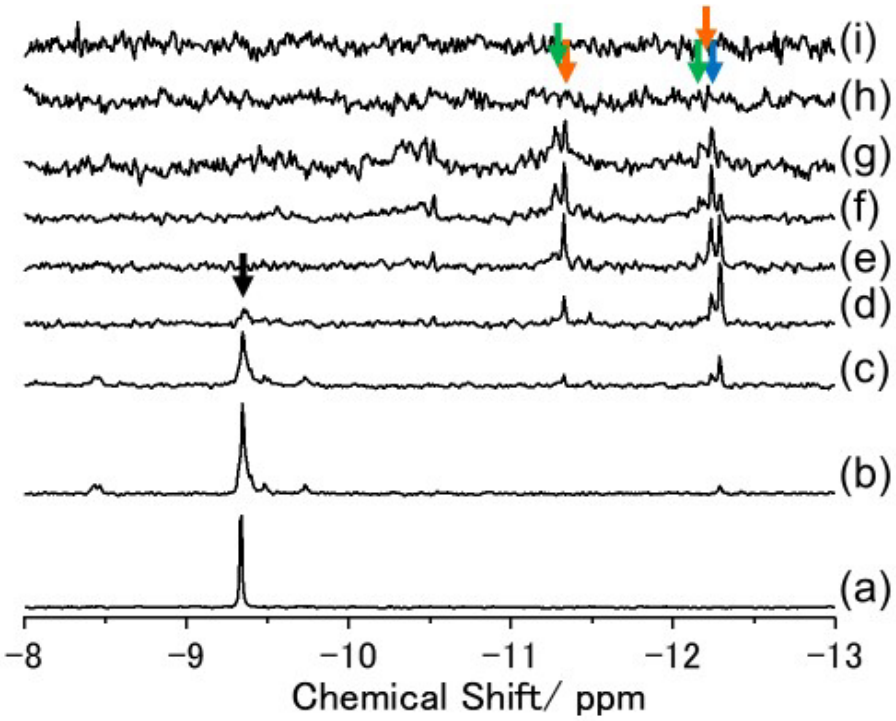

Figure S7. ^{31}P NMR spectra of the filtrate solution after the 2nd recrystallization with different Na_2WO_4:Na_2MoO_4 ratios of (a) 30:0, (b) 27:3, (c) 25:5, (d) 22:8, (e) 20:10, (f) 17:13, (g) 9:21, (h) 3:27, and (i) 0:30 in the reaction mixture; the black (−9.34 ppm), blue (−12.33 ppm), orange (−11.27 and −12.29 ppm) and green (−11.33 and −12.23 ppm) arrows correspond to $[P_5W_{30}O_{110}Na(H_2O)]^{14-}$, $[P_2W_{18}O_{62}]^{6-}$, $[\alpha_2\text{-}P_2W_{17}MoO_{62}]^{6-}$, and $[\alpha_1\text{-}P_2W_{17}MoO_{62}]^{6-}$, respectively.

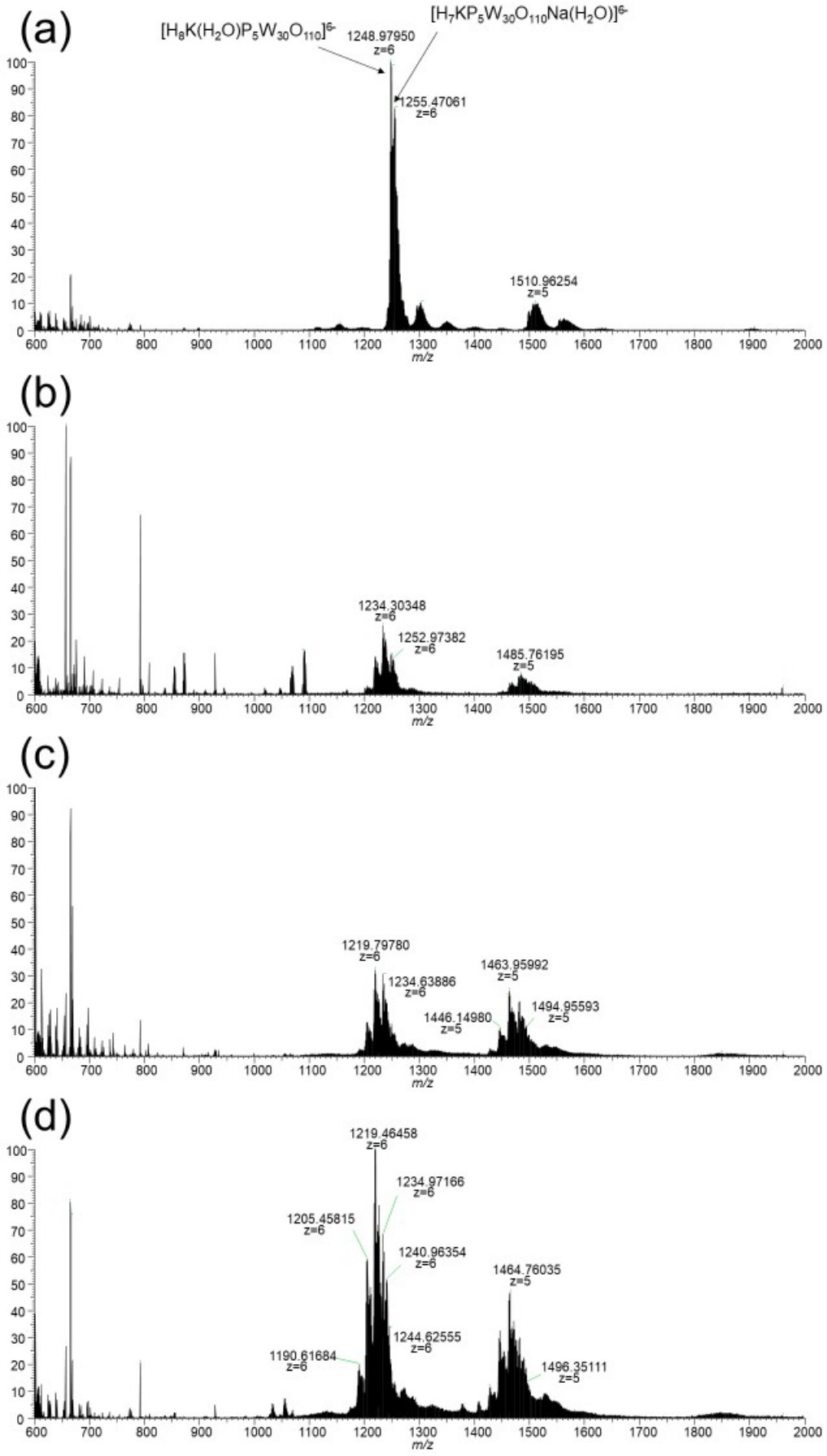
(a)
[H8K(H2O)P5W30O110]6-
[H7KP5W30O110Na(H2O)]6-
1248.97950
z=6
1255.47061
z=6
1510.96254
z=5
(b)
1234.30348
z=6
1252.97382
z=6
1485.76195
z=5
(c)
1219.79780
z=6
1234.63886
z=6
1446.14980
z=5
1463.95992
z=5
1494.95593
z=5
(d)
1219.46458
z=6
1234.97166
z=6
1205.45815
z=6
1240.96354
z=6
1464.76035
z=5
1244.62555
z=6
1190.61684
z=6
1496.35111
z=5
m/z

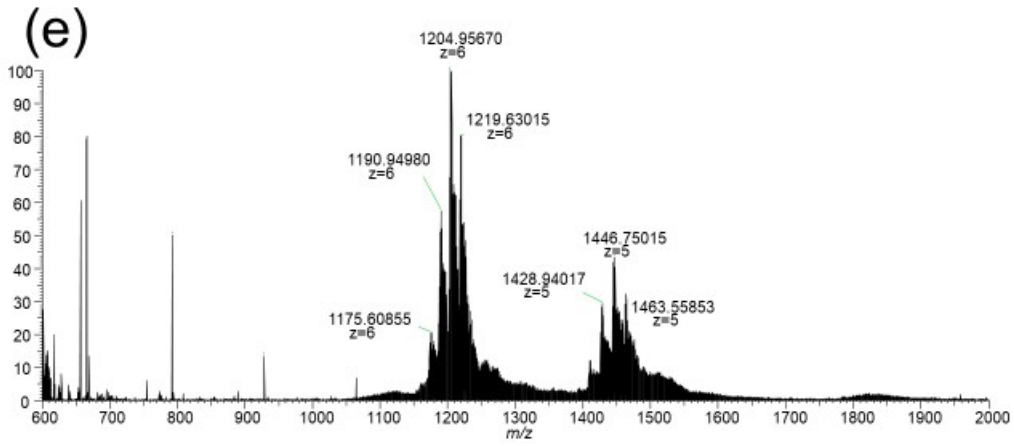

Figure S8. ESI-MS Profile of the Mo-substituted Preyssler-type phosphotungstates with different Mo ratios (a) W:Mo = 30:0, (b) W:Mo = 28.9:1.1, (c) W:Mo = 27.9:2.1, (d) W:Mo = 27.6:2.4, and (e) W:Mo = 25.4:4.6; the sample was dissolved in H_2O/CH_3OH.

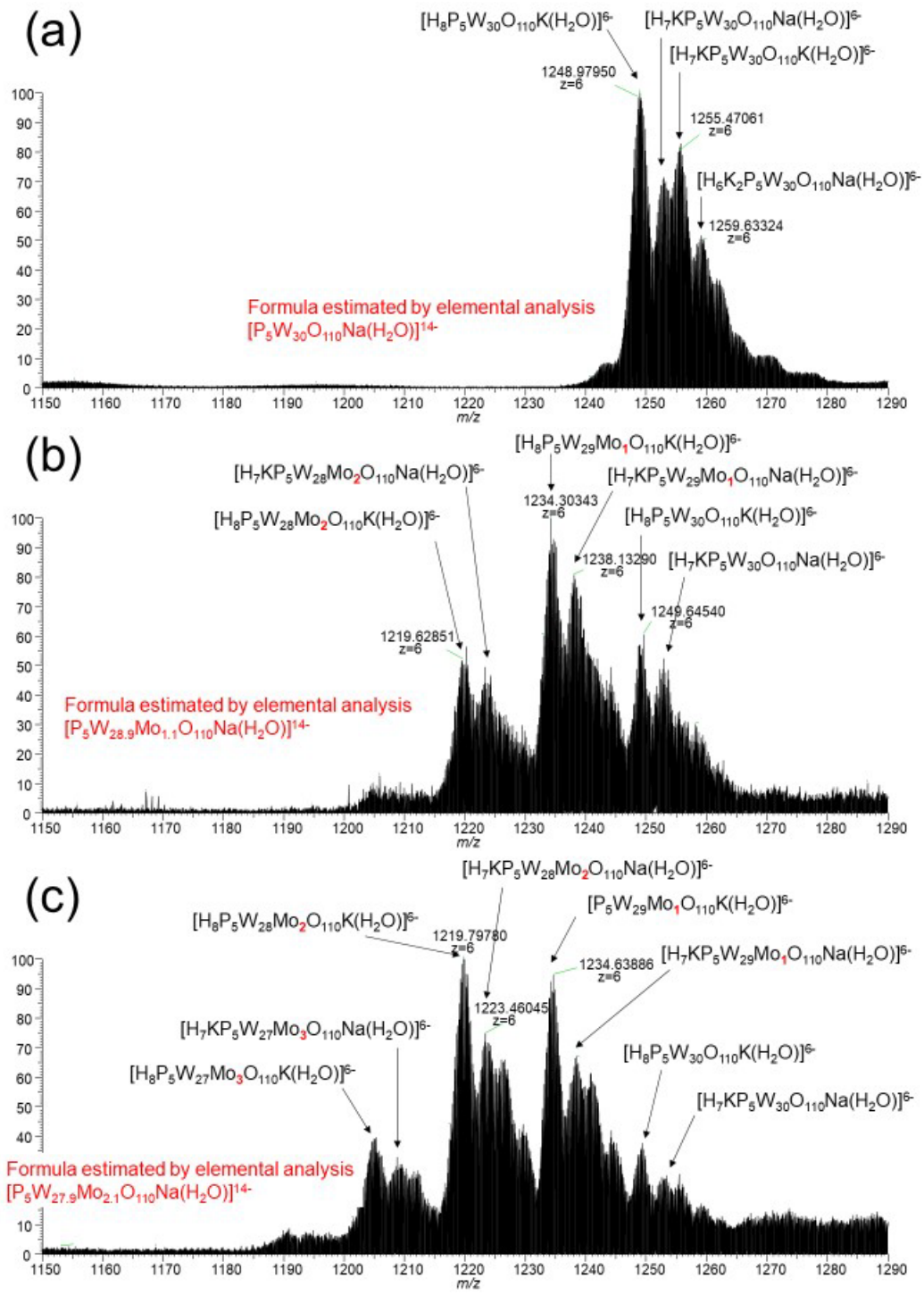
(a)
[H8P5W30O110K(H2O)]6-
[H7KP5W30O110Na(H2O)]6-
[H7KP5W30O110K(H2O)]6-
1248.97950
z=6
1255.47061
z=6
[H6K2P5W30O110Na(H2O)]6-
1259.63324
z=6
Formula estimated by elemental analysis
[P5W30O110Na(H2O)]14-
m/z
(b)
[H8P5W29Mo1O110K(H2O)]6-
[H7KP5W28Mo2O110Na(H2O)]6-
[H7KP5W29Mo1O110Na(H2O)]6-
1234.30343
z=6
[H8P5W28Mo2O110K(H2O)]6-
[H8P5W30O110K(H2O)]6-
1238.13290
z=6
[H7KP5W30O110Na(H2O)]6-
1249.64540
z=6
1219.62851
z=6
Formula estimated by elemental analysis
[P5W28.9Mo1.1O110Na(H2O)]14-
m/z
(c)
[H7KP5W28Mo2O110Na(H2O)]6-
[P5W29Mo1O110K(H2O)]6-
[H8P5W28Mo2O110K(H2O)]6-
1219.79780
z=6
1234.63886
z=6
[H7KP5W29Mo1O110Na(H2O)]6-
1223.46045
z=6
[H7KP5W27Mo3O110Na(H2O)]6-
[H8P5W30O110K(H2O)]6-
[H8P5W27Mo3O110K(H2O)]6-
[H7KP5W30O110Na(H2O)]6-
Formula estimated by elemental analysis
[P5W27.9Mo2.1O110Na(H2O)]14-
m/z

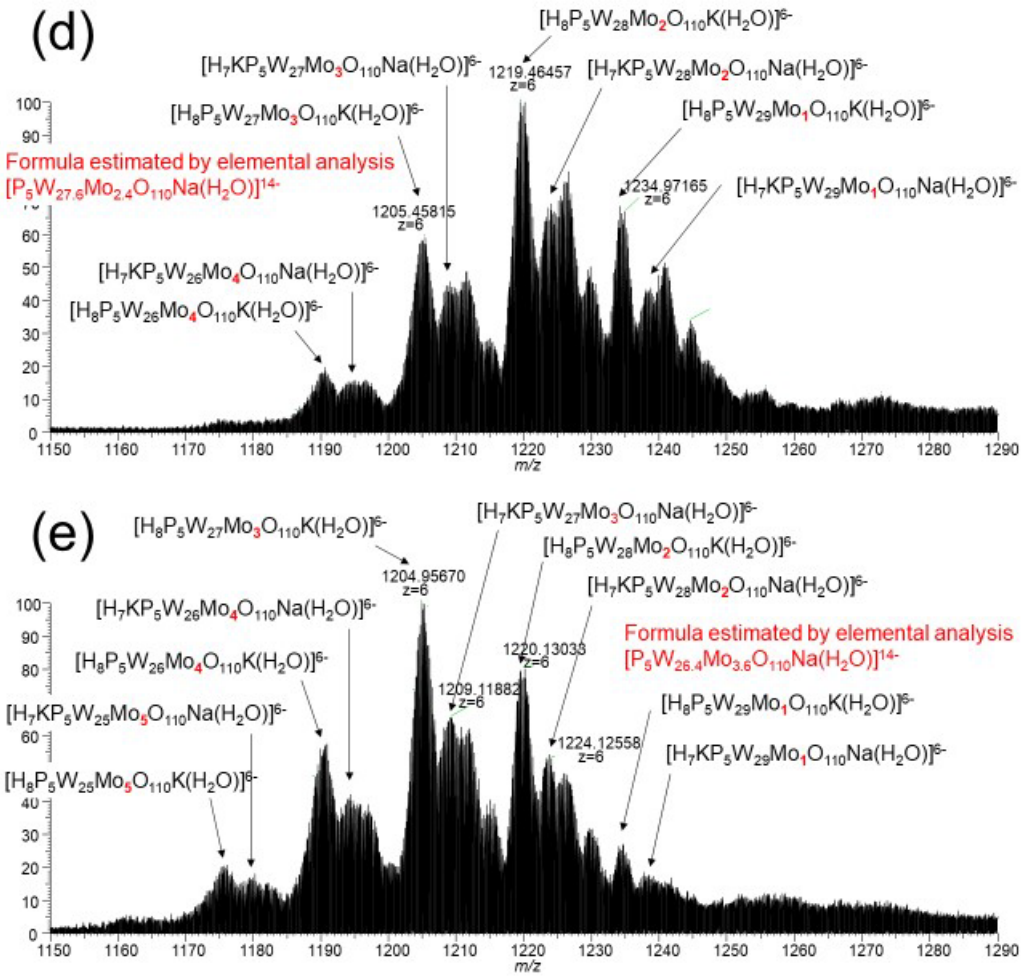

Figure S9. Enlarged (m/z = 1150-1290) ESI-MS Profile of Figure S8. Mo-substituted Preyssler-type phosphotungstates with different Mo ratios (a) W:Mo = 30:0, (b) W:Mo = 28.9:1.1, (c) W:Mo = 27.9:2.1, (d) W:Mo = 27.6:2.4, and (e) W:Mo = 26.4:3.6; the sample was dissolved in H_2O/CH_3OH.

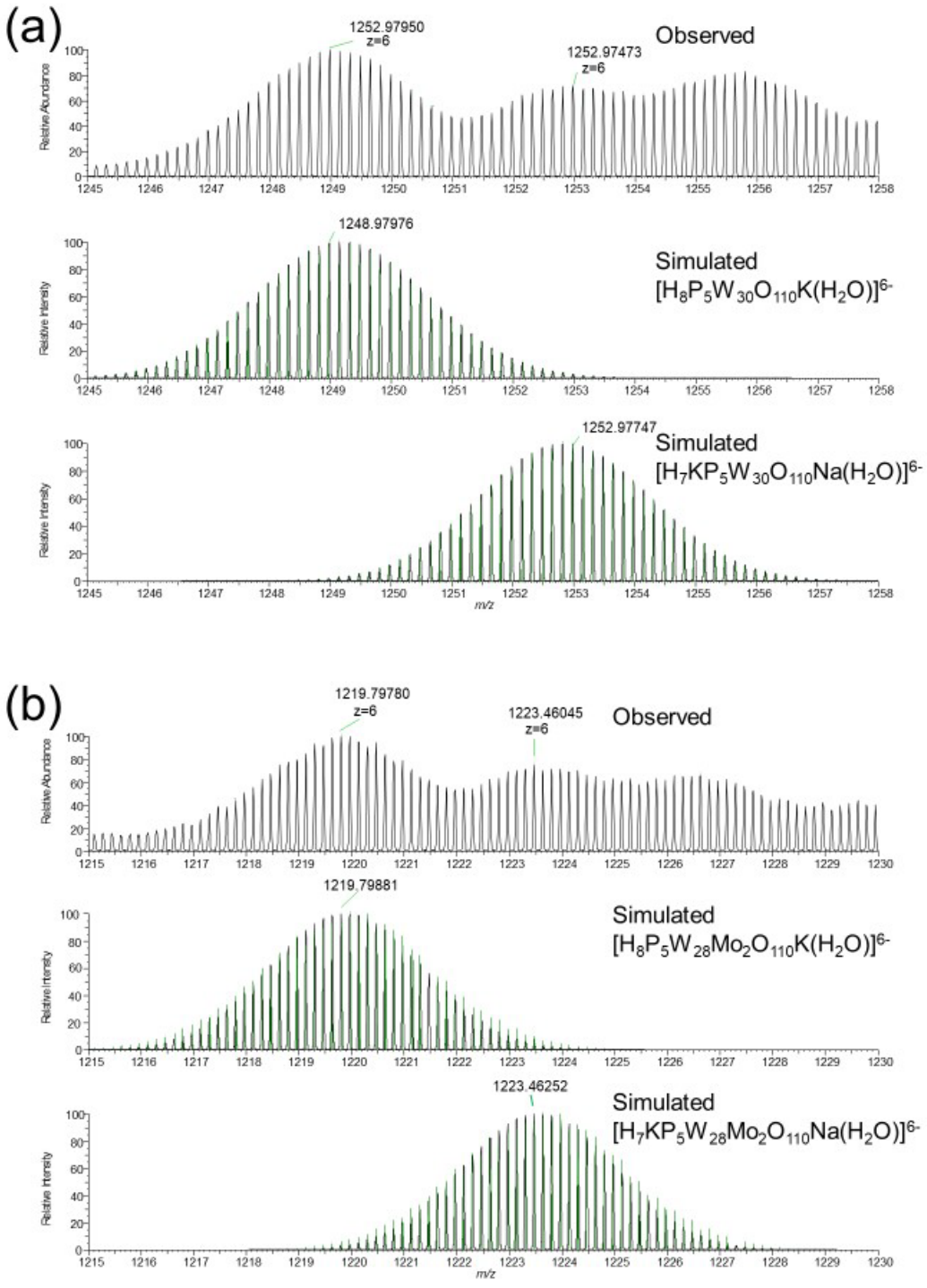

Figure S10. (a) Enlarged ESI-MS spectra of $K_{13}[P_5W_{30}O_{110}Na(H_2O)]$ (Figure S9(a)) with the simulated profile of (middle) $[H_8KP_5W_{30}O_{110}K(H_2O)]^{6-}$ and (lower) $[H_7KP_5W_{30}O_{110}Na(H_2O)]^{6-}$, and (b) the enlarged ESI-MS spectra of

$K_{12.5}Na_{1.5}[P_5W_{27.4}Mo_{2.6}O_{110}Na(H_2O)]$ (Figure 4 and Figure S9(c)) with the simulated profile of (middle) $[H_8KP_5W_{28}Mo_2O_{110}K(H_2O)]^{6-}$ and (lower) $[H_7KP_5W_{28}Mo_2O_{110}Na(H_2O)]^{6-}$.

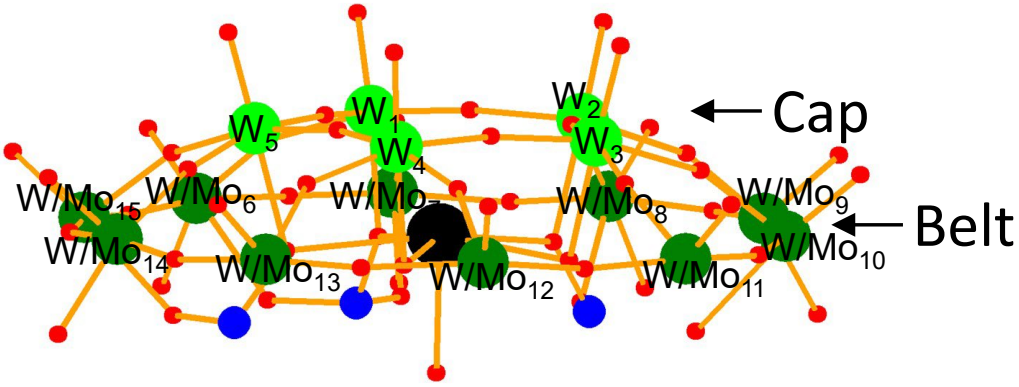

Figure S11. Balls-and-sticks representation of half of the Preyssler molecule found in an asymmetric unit cell; [color codes: light green, W; dark green, W or Mo; blue, P; black, Na; red, O]

Table S1. Site occupancies of W and Mo atoms on the metal centers in a single crystal of $K_{12}Na_2[P_5W_{26.5}Mo_{3.5}O_{110}Na(H_2O)]$.

Atom	Site occupancies (W / Mo)
W_1	1
W_2	1
W_3	1
W_4	1
W_5	1
W_6/Mo_6	0.952(7) / 0.048(1)
W_7/Mo_7	0.946(7) / 0.054(1)
W_8/Mo_8	0.935(7) / 0.065(1)
W_9/Mo_9	0.929(7) / 0.071(1)
W_{10}/Mo_{10}	0.933(7) / 0.067(1)
W_{11}/Mo_{11}	0.946(7) / 0.054(1)
W_{12}/Mo_{12}	0.953(7) / 0.047(1)
W_{13}/Mo_{13}	0.959(7) / 0.041(1)
W_{14}/Mo_{14}	0.945(7)/ 0.055(1)
W_{15}/Mo_{15}	0.940(7) / 0.060(1)

Table S2. Crystallographic table of $K_{12.5}Na_{1.5}[P_5W_{26.4}Mo_{3.6}O_{110}Na(H_2O)]$.

	$K_{12.5}Na_{1.5}[P_5W_{26.4}Mo_{3.6}O_{110}Na(H_2O)]$
CSD No.	2195592
Formula	$H_{78}K_{12}Mo_{1.12}Na_3O_{149}P_5W_{28.88}$
Color, form	colorless, block
Wavelength/ Å	0.41260
Crystal system	Orthorhombic
Space group	*Pnna*
a/ Å	32.8786(7)
b/ Å	21.4959(5)
c/ Å	19.1401(5)
V/ $Å^3$	13527.4(6)
Z	4
T/ K	100(2)
F(000)	15160
ρ calcd/ g· cm^{-3}	4.209
$\mu(\lambda)$/ mm^{-1}	6.130
Crystal size/ mm^3	0.18 × 0.16 × 0.08
Limiting indices	$-39 \le h \le 39$
	$-25 \le k \le 23$
	$-19 \le l \le 23$
R_1 ($I>2\sigma(I)$)[a)]	0.0460
Rw_2 (all data) [b)]	0.1169
GOF	1.156